

Halogenated Benzimidazole Carboxamides Target Integrin $\alpha_4\beta_1$ on T-Cell and B-Cell Lymphomas

Richard D. Carpenter¹, Arutselvan Natarajan², Edmond Y. Lau⁴, Mirela Andrei³, Danielle M. Solano¹, Felice C. Lightstone⁴, Sally J. DeNardo², Kit S. Lam³, and Mark J. Kurth¹

Abstract

Integrin $\alpha_4\beta_1$ is an attractive but poorly understood target for selective diagnosis and treatment of T-cell and B-cell lymphomas. This report focuses on the rapid microwave preparation, structure-activity relationships, and biological evaluation of medicinally pertinent benzimidazole heterocycles as integrin $\alpha_4\beta_1$ antagonists. We documented tumor uptake of derivatives labeled with ¹²⁵I in xenograft murine models of B-cell lymphoma. Molecular homology models of integrin $\alpha_4\beta_1$ predicted that docked halobenzimidazole carboxamides have the halogen atom in a suitable orientation for halogen-hydrogen bonding. The high-affinity halogenated ligands identified offer attractive tools for medicinal and biological use, including fluoro and iodo derivatives with potential radiodiagnostic (¹⁸F) or radiotherapeutic (¹³¹I) applications, or chloro and bromo analogues that could provide structural insights into integrin-ligand interactions through photoaffinity, cross-linking/mass spectroscopy, and X-ray crystallographic studies. *Cancer Res*; 70(13); 5448–56. ©2010 AACR.

Introduction

Current cancer chemotherapeutic agents aim to annihilate tumors through mechanisms such as DNA alkylation, unnatural base pair recognition, inhibition of topoisomerases, and microtubule stabilization mechanisms. However, these agents have a narrow therapeutic index, are administered near their maximum tolerated dose, and are largely nondiscriminatory in recognizing either normal or cancerous cells. As a consequence, patients suffer from serious side effects including neutropenia, thrombocytopenia, neuropathy,

nausea, vomiting, diarrhea, hair loss, anemia, and various organ toxicities. Although significant effort has been directed through lengthy syntheses of complex cytotoxic natural products, not until recently has attention been focused towards target-selective chemotherapeutics that could reduce off-target binding and ensuing side effects (1).

The resting or activated conformations of $\alpha_4\beta_1$ integrin allow for the application of target-selective agents for malignant lymphoid cancers; activated $\alpha_4\beta_1$ integrin is expressed on leukemias, lymphomas, melanomas, and sarcomas (2, 3). Integrins are heterodimeric transmembrane receptor proteins crucial for cell-cell, cell-matrix, and cell-pathogen interactions (4). Integrin $\alpha_4\beta_1$ plays an important role in autoimmune diseases and inflammation (5), as well as tumor growth, angiogenesis, and metastasis (6–11). Indeed, $\alpha_4\beta_1$ integrin facilitates tumor cell extravasation (6), prevents apoptosis of malignant B-chronic lymphocytic leukemia cells (7), is key to drug resistance in both multiple myeloma and acute myelogenous leukemia (8), and has been selectively targeted with peptidomimetics (3, 12–16). Nonetheless, $\alpha_4\beta_1$ integrin has not garnered much attention as either a therapeutic or a diagnostic cancer target due to the lack of potent and specific agents.

In accord with our program to discover potent and selective ligands that target various cancers, we have developed two *in vivo* imaging agents that have been successful in murine models (3, 12–17). Figure 1A and B show the structure of these agents; the bisaryl urea 1-Cy5.5 (LLP2A-Cy5.5; Fig. 1A; refs. 3, 14) and the benzothiazole analogue 2-Cy5.5 (KLCA14-Cy5.5; Fig. 1B; ref. 15), both showed high affinity and specificity for B- and T-cell lymphomas containing activated $\alpha_4\beta_1$ integrin, with the latter showing improved tumor/kidney signal. This is likely due to the

Authors' Affiliations: ¹Department of Chemistry, University of California, Davis, Davis, California; ²Divisions of Hematology and Oncology, and Radiodiagnosis and Therapy, Department of Internal Medicine, U.C. Davis Cancer Center, University of California, Davis School of Medicine, Sacramento, California; ³Division of Hematology and Oncology, Department of Internal Medicine, U.C. Davis Cancer Center, University of California, Davis, School of Medicine, Sacramento, California; and ⁴Physical and Life Sciences Directorate, Lawrence Livermore National Laboratory, Livermore, California

Note: Supplementary data for this article are available at Cancer Research Online (<http://cancerres.aacrjournals.org/>).

K.S. Lam and M.J. Kurth share senior authorship.

Current address for R.D. Carpenter: Department of Biomedical Engineering, Genome and Biomedical Sciences Facility, University of California, Davis, Davis, CA.

Current address for A. Natarajan: Molecular Imaging Program at Stanford, Department of Radiology, Stanford University, Stanford, CA.

This research is dedicated in remembrance of our former colleague Professor Aaron D. Mills (University of Idaho).

Corresponding Author: Mark J. Kurth, Department of Chemistry, University of California, Davis, Davis, CA 95616. Phone: 530-554-2145; Fax: 530-752-8895; E-mail: mjkurth@ucdavis.edu.

doi: 10.1158/0008-5472.CAN-09-3736

©2010 American Association for Cancer Research.

improved solubility of 2-arylaminoazole heterocycle (13, 15) over the bisaryl urea as these heterocycles have a lower log *P*, a higher dipole moment, and an increased acidity of the 2-arylamino N-H ($pK_a = 5.5$ – 6.5 ; ref. 18). However, both **1-Cy5.5** and **2-Cy5.5** have approximately one third of the molecular weight committed to the $\alpha_4\beta_1$ integrin-targeting motif with the rest of the molecular weight devoted to the linker and the dye. Furthermore, due to the limited range of tissue penetration, optical imaging is not practical for whole-body imaging in humans. There is a need to develop a condensed $\alpha_4\beta_1$ integrin radiotargeting agent that could not only be used for positron emission tomography and single-photon emission computed tomography imaging but also for radiotherapy. With efforts integrating heterocyclic chemistry, cell adhesion assays, molecular modeling, and radiochemistry, we report herein the discovery of the bromobenzimidazole carboxamide **5** ($IC_{50} = 115$ pmol/L), the structure-activity relationship between halobenzimidazole carboxamides **3** to **6**, and the biological evaluation of radioiodinated derivatives **7**, **8**, and **18** (structures shown in Fig. 1C and D).

Materials and Methods

Chemical synthesis

Compounds **3** to **9**, **11** to **13**, and **16** and **17** were synthesized as outlined in Supplementary Schemes 1 to 4. Compounds **1** and **2** (as well as **1-Cy5.5** and **2-Cy5.5**), **9**, **14**, and **15a** and **b** have been previously reported (3, 13, 15, 19, 20). The synthesis of **3** to **6** was analogous to our previous work (15); however, the analytical data for these compounds is listed below. The synthesis of **7** and **8**, **10** to **13**, and **16** to **21** is described below.

(S)-6-(1-Carbamoylcyclohexyl-amino)-5-[(S)-2-{4-(5-fluoro-1H-benzo[d]imidazol-2-yl)amino}-benzamido]-6-[(E)-3-(pyridin-3-yl-acrylamido)hexanamido]-6-oxo-hexanoic acid (**3**)

Following our procedure for benzimidazole analogues (15) afforded **3** as a white solid (10 mg, 44%); ESI-MS (*m/z*) 798.8 ($M + H$)⁺, ESI-HRMS for $C_{41}H_{49}FN_9O_7$ ($M + H$)⁺: calcd, 798.3733; found, 798.4481 (*m/z*). Purity was determined to

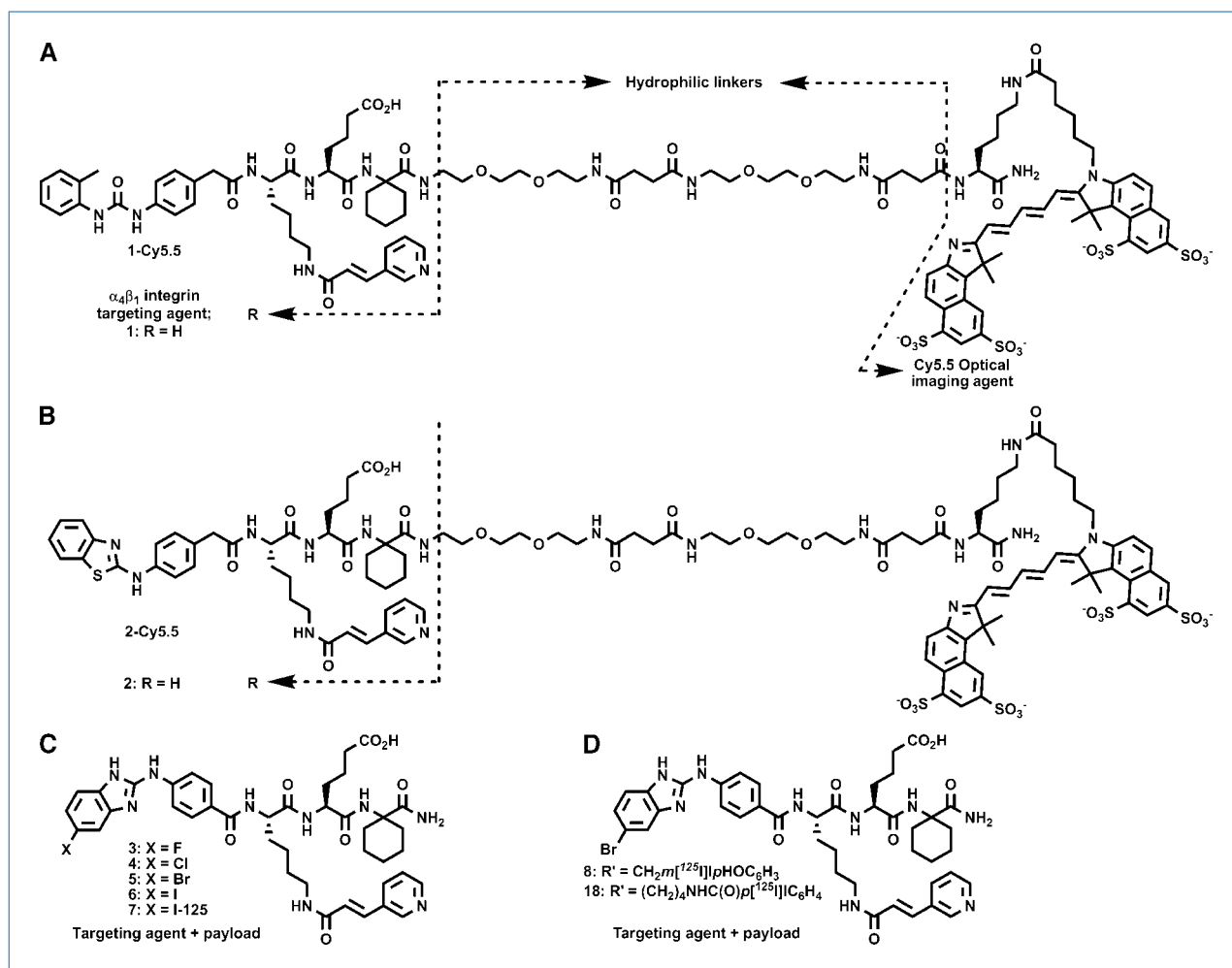


Figure 1. Structures of: (A) **1-Cy5.5** (**3**), (B) **2-Cy5.5** (**15**), (C) halobenzimidazole analogues **3** to **7**, and (D) the bishalo analogues **8** and **18**, which incorporate the bromobenzimidazole moiety and a distal radiiodide.

be 96% as determined by analytic high-performance liquid chromatography (HPLC).

(S)-6-(1-Carbamoylcyclohexylamino)-5-[(S)-2-{4-(5-chloro-1H-benzo[d]imidazol-2-ylamino)-benzamido}-6-[(E)-3-(pyridin-3-yl)acrylamido}hexanamido]-6-oxo-hexanoic acid (4)

Following our procedure for benzimidazole analogues (15) afforded **4** as a white solid (22 mg, 57%): ESI-MS 814.3, 816.3 (m/z) ($M + H$)⁺, ESI-HRMS for C₄₁H₄₉ClN₉O₇ ($M + H$)⁺: calcd, 814.3438; found, 814.2894 (m/z). Purity (HPLC), 96%.

(S)-5-[(S)-2-{4-(5-Bromo-1H-benzo[d]imidazol-2-ylamino)benzamido}-6-[(E)-3-(pyridin-3-yl)acrylamido}hexanamido]-6-(1-carbamoylcyclohexylamino)-6-oxo-hexanoic acid (5)

Following our procedure for benzimidazole analogues (15) afforded **5** as a white solid (28 mg, 39%): ESI-MS (m/z) 858.4, 860.6 ($M + H$)⁺, ESI-HRMS for C₄₁H₄₉BrN₉O₇ ($M + H$)⁺: calcd, 906.2794; found, 906.2843 (m/z). Purity (HPLC), 99%.

(S)-6-(1-Carbamoylcyclohexylamino)-5-[(S)-2-{4-(5-iodo-1H-benzo[d]imidazol-2-ylamino)benzamido}-6-[(E)-3-(pyridin-3-yl)acrylamido}hexanamido]-6-oxo-hexanoic acid (6)

Following our procedure for benzimidazole analogues (15) afforded **6** as a white solid (18 mg, 48%): ESI-MS 906.3 (m/z) ($M + H$)⁺, ESI-HRMS for C₄₁H₄₉IN₉O₇ ($M + H$)⁺: calcd, 906.2794; found, 906.2843 (m/z). Purity (HPLC), 96%.

[¹²⁵I]-[(S)-6-(1-Carbamoylcyclohexylamino)-5-[(S)-2-{4-(5-iodo-1H-benzo[d]imidazol-2-ylamino)benzamido}-6-[(E)-3-(pyridin-3-yl)acrylamido}hexanamido]-6-oxo-hexanoic acid (7)

Radioiodination of the compound bromobenzimidazole carboxamide **5** using Na¹²⁵I was evaluated by a number of methods and conditions but the following procedure provided the most consistent and best yields. Briefly, 50 μL of a 2.5 mmol/L solution of compound **5** in 1 mol/L of sodium phosphate (pH 7.0) was added to 50 μL of a 5 mol/L solution of chloramine T in distilled water and mixed in a vial containing 185 MBq of Na¹²⁵I and 10 mol% of CuI at 50°C for 20 minutes. This mixture was then quenched with 100 μL of 5 mmol/L sodium bisulfite for about 15 minutes. Radiolabeled **7** was eluted through a C₁₈ spin column with 250 μL of 1:1 acetonitrile/water. Radiolabeling yields were in the range of 20% to 25%, with specific activities ranging from 25.4 to 38.0 MBq (0.8–1.2 μCi)/μmol (specific activity was calculated and corrected after final purification). Quality assurance for compound **7** was estimated by reverse-phase HPLC (RP-HPLC) with radioactive and UV detectors and the labeled peptide showed a single peak of >95% purity. The final purified products showed >95% monomeric compounds by C₁₈ TLC, RP-HPLC, and CAE runs of 11 and 45 minutes; the unbound radioiodine was <5%.

[¹²⁵I]-[(S)-6-[1-[(S)-3-Amino-2-(4-hydroxy-3-iodobenzyl)-3-oxopropanoyl-carbamoyl]cyclohexylamino]-5-[(S)-2-{4-(5-bromo-1H-benzo[d]imidazol-2-ylamino)benzamido}-6-[(E)-3-(pyridin-3-yl)acrylamido}hexanamido]-6-oxo-hexanoic acid (8)

A 2.5 mmol/L solution of compound **5** (200 μg, 50 μL) in 1 mol/L of sodium phosphate (adjusted to pH 7.0 with H₃PO₄) was added to 50 μL of a 5 mmol/L solution of chloramine T in DMSO (200 μL) and mixed in a vial containing Na¹²⁵I (1 mCi, 10 μL), 10 mol% diethyldiamine and 10 mol % ratio of CuI at 50°C for 20 minutes. After 20 minutes, this mixture was quenched with 100 μL of a 5 mmol/L solution of NaHSO₃ in H₂O for 15 minutes. Crude radiolabeled **8** was eluted through a C-18 spin column with 250 μL of 1:1 acetonitrile/water to afford pure **8** in 90% radiochemical yield, with specific activities ranging from 25.4 to 38.0 MBq (2 μCi)/μg, and >95% purity. The final purified products showed >95% monomeric compounds by C-18 TLC, RP-HPLC, and CAE runs of 11 and 45 minutes; the unbound radioiodine was <5%.

General procedure for halobenzimidazole acids: 4-(5-fluoro-1H-benzo[d]imidazol-2-ylamino)benzoic acid (10)

Our previously reported methods (15) were used with the following exceptions: a sealable microwave tube was used as the reaction vessel and after the consumption of **9** as determined by TLC, 1,3-diisopropylcarbodiimide (451 μL, 2.90 mmol) was added, the tube was sealed, and the reaction mixture was microwave-heated to 80°C for 11 minutes. After our previously described workup, this crude ester was then dissolved in DMF (8 mL), transferred to a sealable microwave tube, treated with Ba(OH)₂ (1.65 g, 9.65 mmol), and microwave-heated to 140°C for 21 minutes. The mixture was filtered as previously described to afford **10** (225 mg, 86%) as a gray solid: ESI-MS (m/z) 272 ($M + H$)⁺. Purity (HPLC), 98%.

4-(5-Chloro-1H-benzo[d]imidazol-2-ylamino)benzoic acid (11)

Following the general procedure for halobenzimidazole acids afforded **11** as a gray solid (249 mg, 89%): ESI-MS (m/z) 288, 290 ($M + H$)⁺. Purity (HPLC), 99%.

4-(5-Bromo-1H-benzo[d]imidazol-2-ylamino)benzoic acid (12)

Following the general procedure for halobenzimidazole acids afforded **12** as a gray solid (205 mg, 64%): ESI-MS (m/z) 332, 334 ($M + H$)⁺; found C, 50.70; H, 3.03; N, 12.63. Purity (HPLC), 100%.

4-(5-Iodo-1H-benzo[d]imidazol-2-ylamino)benzoic acid (13)

Following the general procedure for halobenzimidazole acids afforded **13** as a brown solid (275 mg, 75%): ESI-MS (m/z) 380.0 ($M + H$)⁺. Purity (HPLC), 97%.

(S)-6-[1-((S)-3-Amino-2-(4-hydroxybenzyl)-3-oxopropanoylcarbamoyl)cyclohexyl-amino]-5-[(S)-2-(4-(5-bromo-1H-benzo[d]imidazol-2-ylamino)benzamido)-6-[(E)-3-(pyridin-3-yl)acrylamido]-hexanamido]-6-oxohexanoic acid (17)

Our previously reported methods (15) afforded first **16** and then **17** as a yellow solid (6 mg, 4.9%); ESI-MS 1023.69 (m/z) ($M + H$)⁺. Purity (HPLC), 91%.

[¹²⁵I]-((S)-6-[1-((S)-1-Amino-6-(4-iodobenzamido)-1-oxohexan-2-ylcarbamoyl)-cyclohexyl-amino]-5-[(S)-2-(4-(5-bromo-1H-benzo[d]imidazol-2-ylamino)benz-amido)-6-[(E)-3-(pyridin-3-yl)acrylamido]-hexanamido]-6-oxohexanoic acid (18)

Amine **21** (50 μ g, 41.2 μ mol) and *N*-succinimidyl-4-[¹²⁵I]iodobenzoate (14 μ g, 41.2 μ mol, 200 μ Ci; ref. 21) in alkaline water (pH 8.0) was warmed to 60°C for 1 hour. Crude **18** was eluted through C₁₈ spin column with 250 μ L of 1:1 acetonitrile/water to afford pure **18** in 47% radiochemical yield, with a specific activity of 1.7 μ Ci/g, and >95% purity. Purity (C₁₈ TLC and RP-HPLC), >90%.

(S)-5-((S)-2-(4-(5-Bromo-1H-benzo[d]imidazol-2-ylamino)benzamido)-6-[(E)-3-(pyridin-3-yl)acrylamido]-hexanamido)-6-(1-((S)-1,6-diamino-1-oxohexan-2-ylcarbamoyl)cyclohexylamino)-6-oxohexanoic acid (21)

Our previously reported methods (15) afforded **21** (4.9 mg, 4.2%) as a white powder: ESI-MS 988.46 (m/z) ($M + H$)⁺. Purity (HPLC), 100%.

Multiple sequence alignment and model building

The sequence alignment between $\alpha_4\beta_1$ integrin and the template ($\alpha_{11b}\beta_3$ integrin; ref. 22; see Supplementary Figs. S3–4) was performed using PSI-BLAST-ISS (23). Sequences having similarity to both $\alpha_4\beta_1$ and $\alpha_{11b}\beta_3$ integrins were used as seeds to generate corresponding PSI-BLAST profiles (24), which were extracted and compared. Protein models were generated using MODELLER (25).

Docking simulations

Compounds were docked in the vicinity of Trp188 in (α_4) using Autodock (26). The partial atomic charges for the ligands were obtained using the AM1-BCC (27) method and united atom charges were used for the integrin (28). An 80 × 90 × 90 \AA grid was used with a spacing of 0.375 \AA and centered above Trp188. A Lamarckian algorithm was used to generate ligand conformations using previously reported parameters whereas keeping the energy evaluations at a maximum of 150,000 (29). A total of 5,000 conformers were generated for each ligand and clustered using a 2.0 \AA root mean square deviation.

Cell adhesion assay

The cell adhesion assay method is described elsewhere (13, 15).

Animal biodistribution study for 7

Eleven female BALB/c *nu/nu* mice, 5 to 6 weeks old (U.C. Davis Animal Care Facility), were xenografted s.c. in the abdomen with 5×10^6 Raji cells. Three weeks after inoculation, the tumor size of the mice was measured. The mice were injected i.v. with 4 to 6 μ Ci of ¹²⁵I-labeled **7** (5 μ g, 6 nmol) with normal saline as the vehicle. The mice were sacrificed at 4, 24, and 48 hours postinjection and tissue samples were excised. The tissue samples were weighed and radioactivity was measured in a gamma counter. Uptake in harvested organs was expressed as % ID/g of tissue.

Animal biodistribution study for 18

Six female BALB/c *nu/nu* mice, 5 to 6 weeks old (U.C. Davis Animal Care Facility), were xenografted s.c. in the abdomen with 6×10^6 Raji cells. Three weeks after inoculation, the tumor size of the mice was measured. The mice were injected i.v. with **18** (5 μ g, 4 nmol, 12 μ Ci specific activity) with normal saline as the vehicle. Three mice were sacrificed at 24 hours postinjection and the other three at 48 hours postinjection, and tissue samples were excised. The tissue samples were weighed and radioactivity was measured in a gamma scintillation counter. Uptake in harvested organs was expressed as % ID/g of tissue.

Results and Discussion

Chemistry

Both the azole carboxamide and bromoazole acetamide series were previously known to be ineffective ligands for $\alpha_4\beta_1$ integrin. Indeed, previous structure-activity relationship studies found that a methylene unit between the amide and the phenyl ring (i.e., arylacetamide) was believed to be a critical motif for potency (3), whereas bromo substitution was ineffective at increasing potency (13, 15). Nonetheless, molecular modeling studies revealed a channel near the ligand binding site where a halogen atom could potentially interact (15). Halogenated ligands are all particularly attractive for use in medicine and biology as either a radiodiagnostic (¹⁸F), a radiotherapeutic (¹³¹I), or a molecular structure tool (Cl or Br). In the latter example, either chloro or bromo ligands could be used to provide valuable molecular insight into the integrin structure in either photoaffinity cross-linking/mass spectroscopy experiments (Cl, 3:1 ³⁵Cl:³⁷Cl; Br, 1:1 ⁷⁹Br:⁸¹Br), as well as cocrystallization X-ray studies (heavy atom effect). This provided the impetus behind the synthesis of halobenzimidazole analogues **10** to **13** (Supplementary Scheme 1).

Although milder tandem reactions have been recently developed to afford *m*- and *p*-azole esters in good yields (30, 31), the reaction conditions shown in Supplementary Scheme 1 quarter the amount of time to deliver halobenzimidazole acids **10** to **13** through microwave-mediated chemistry (32). Briefly, commercially available aniline esters were treated with thiophosgene to afford the aryl isothiocyanate ester **9** in 83% yield. Following purification by short path column chromatography, this aryl isothiocyanate ester

was reacted with 4-halo-*o*-phenylenediamine to yield an intermediate bisaryl thiourea that, in the presence of 1,3-diisopropylcarbodiimide, was cyclized to yield crude benzimidazole esters and 1,3-diisopropylthiourea as a by-product. These esters are rapidly saponified to afford halobenzimidazole acids **10** to **13** (64–89% yield) that are analytically pure following acidification and filtration (33). This streamlined route, coupled with previous reports focusing on milder reagents and conditions that minimize purification (15, 30), significantly

improves the preparation of these medically pertinent azole heterocycles which are present in nearly one-quarter of the top 100 drugs (34).

With these halobenzimidazole acids in hand, effort was then directed towards the synthesis of target molecules **3** to **6** (Supplementary Scheme 2). The tripeptide **14**, prepared previously from Rink amide resin (13), was *N*-acylated with halobenzimidazole acid precursors **10** to **13**, followed by acid-mediated deprotection and resin cleavage to afford

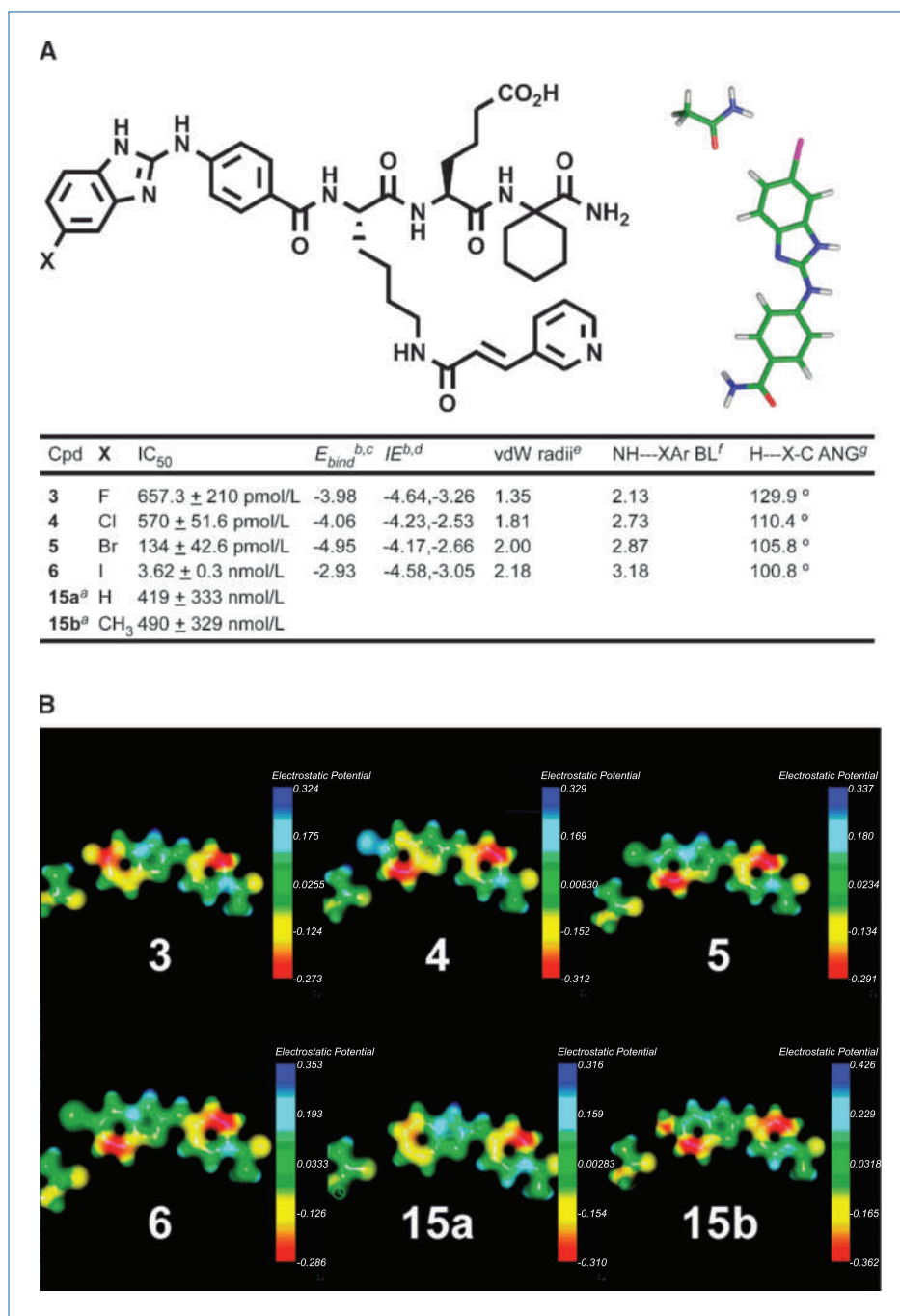


Figure 2. A, potency (IC₅₀), estimated binding energies, calculated interaction energies, and amide-halogen geometries, where the amide represents a nearby primary amide of Asn¹⁶¹ (α_4 subunit) side chain: a, see ref. 13 for more on **15a**, ref. 15 for more on **15b**. b, energies are expressed in units of kcal/mol. c, estimated binding energies (E_{bind}), in which $E_{\text{bind}} = RT \cdot \ln[IC_{50}(X = \text{halogen})/IC_{50}(X = H)]$. d, calculated interaction energy for amide-halogen interaction (gas phase) using MP2/6-311++G(d,p)//B3LYP/6-311++G(d,p) level of theory, second values are the BSSE-corrected energies. e, distances for the van der Waal's (vdW) radii of each halogen are expressed in angstroms. f, distances (in angstroms) represent the C(O)NRH...XAr H-bond length. g, represents the H-X-Ar angle in the C(O)NRH...XAr H-bond. B, electrostatic potential maps for **3** to **6** and **15a** and **15b**.

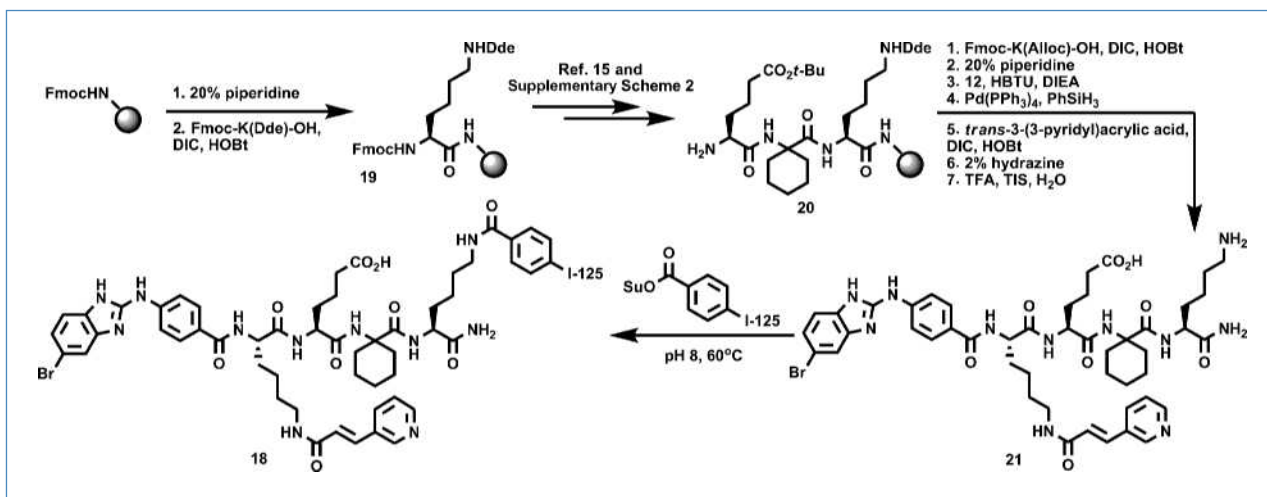


Figure 3. Preparation of **18** from the tyrosine derivative **19**, as described in ref. 15.

crude **3** to **6**. Purification by RP-HPLC and lyophilization delivered pure halobenzimidazole carboxamide analogues **3** to **6** in 22% to 46% overall yield from Rink amide resin.

In vitro biological evaluation

Halobenzimidazole carboxamide analogues **3** to **6** were then subjected to cell adhesion competitive inhibition assays to determine *in vitro* activity and potency. The 25-mer peptide CS-1 (DELPLQLVTLPHPNLHGPEILDVPSST), the binding motif of fibronectin to $\alpha_4\beta_1$ integrin, provides a natural ligand to measure the binding affinities (IC_{50}) of the halobenzimidazole carboxamide analogues **3** to **6**.

Briefly, 96-well plates were coated with neutravidin followed by treatment of biotinylated CS-1 to immobilize the natural ligand to the well of the plate. The remaining non-neutravidin-bound sites were blocked with bovine serum albumin and the wells were incubated with Molt-4 cells (human T-cell leukemia containing $\alpha_4\beta_1$ integrin). The plates were then washed, fixed with formalin, stained with crystal violet, and absorbance (570 nm) was measured using a UV/Vis spectrophotometer equipped to read 96-well plates. Inhibition was calculated as a percentage resulting from the concentration-dependent curve (see Supplementary Materials), with the potency of **3** to **6** shown in Fig. 2A. Although all compounds have an affinity for $\alpha_4\beta_1$ integrin at <5 nmol/L, these data suggest that the type of halogen atom plays a critical role for ultrapotency in this class of halobenzimidazole analogues. The bromo, fluoro, and iodo derivatives are particularly promising; the bromo compound **5** is only 2-fold less potent than previous leads (**4**, **19**), whereas the fluoro (**3**) and iodo (**6**) analogues could potentially be highly potent radiodiagnostic (F-18) and radiotherapeutic (I-131) agents.

Structure-activity relationship and theoretical calculations

Interestingly, the structure-activity relationship for this class of benzimidazole carboxamides (see Fig. 2A) revealed that both the unsubstituted benzimidazole (**15a**; ref. 13) and

5⁶-methylbenzimidazole (**15b**; ref. 15) were 1,000-fold less potent than fluoro, chloro, and bromo analogues **3** to **5** as well as 100-fold less potent than iodo analogue **6**. These data suggest that hydrophobic interactions were not responsible for ultrapotency, as both **15a** and **15b** were equipotent. Additionally, steric interactions were also not responsible, as 1,000-fold difference was seen between isosteres **15a** and **3** as well as **15b** and **4**. Electrostatic interactions were also examined; however, these interactions were not important as the electrostatic potential of **3** to **6** and **15a** and **15b** (see Fig. 2B) did not correlate with the observed potency. Therefore, attention turned towards aryl halide-derived interactions which have occurred in prior systems through aryl halide-H bonding (35) or halogen-carbonyl dipole-dipole interactions (36, 37).

To further understand if the aryl halide-H-bond and/or dipole-dipole interactions were involved, the binding energy (E_{bind}) was estimated for **3** to **6** (see Fig. 2A) using the equation $E_{bind} = RT \cdot \ln[IC_{50}(X = \text{halogen})/IC_{50}(X = H)]$, where R is the gas constant and T is the temperature at 25°C. Quantum mechanical calculations were performed where halobenzimidazoles interacted with primary amide (i.e., Asn/Gln), ammonium (Lys), or carboxylate (Asp/Glu) side chains. Interestingly, only calculations involving the interaction between the primary amide side chain of Asn or Gln with halobenzimidazoles gave results consistent with the experimental observations, thereby eliminating Lys, Asp, and Glu residues as well as charge-transfer interactions. These data suggest that the nature of either the H-bond donor or carbonyl source is critical for ultrapotency.

The nature of the amide-aryl halide interaction was elucidated by investigating the geometries and interaction energies of both the carbonyl oxygen and the amide N-H interacting with the halobenzimidazole. Having the hydrogen N-H interacting with the halogen gave a stabilizing interaction for halobenzimidazoles **3** to **6**. Although the carbonyl oxygen interacting with heavier halo analogues **4** to **6** was stabilizing, it was unfavorable when interacting

with fluoro analogue **3**. The gas phase-calculated interaction energies (IE) were then determined at the MP2/6-311++G(d,p)/B3LYP/6-311++G(d,p) level and ranged from 3.5 to 4.0 kcal/mol as shown in the chart of Fig. 2A. These IE values were primarily due to the H-bond between the primary amide of Asn¹⁶¹ (α_4 subunit) and the halobenzimidazole moiety. The IE values predict that fluoro analogue **3** would be the most potent; however, all IE values are very close (within 0.5 kcal/mol) and were comparable with experimentally observed E_{bind} values. The variation in potency is likely explained by bromo analogue **5** having the halogen with the requisite van der Waal's atomic radii (2.00 Å for Br; ref. 38) and positioning of the halogen atom (105.8° angle of the C(O)NRH...X-Ar H-bond, where X is the central atom of the angle and a halogen, is taken from the minimized energy structures shown generically in Fig. 2A) allowing for this key amide-halogen H-bond (bond length between H...X = 2.87 Å), whereas permitting other moieties to interact with the α_4 and β_1 subunits (such as the butanoate-Mg²⁺ interaction at the MIDAS site of the β_1 subunit; ref. 15). This theory helps explain why the larger iodo analogue **6** (the poorest H-bond acceptor) is approximately 10-fold less potent than the fluoro (**3**), chloro (**4**), and bromo (**5**) analogues and 100-fold more potent than the unsubstituted (**15a**) and methyl analogues (**15b**).

Radioiodination via aromatic Finkelstein and initial biodistribution studies

The condensed radioiodide derivatives **7** and **8** were attractive targets to potentially serve as therapeutic or diagnostic agents for T- and B-cell lymphomas. Radioiodo derivative **7** was particularly attractive, as this could be synthesized from the bromo analogue **5** in a copper-mediated radioiodination (39, 40). Buchwald's copper(I)-mediated aromatic Finkelstein reaction with cold sodium iodide (i.e., ArBr → ArI) that proceeds with average yields of 97% for many aryl and heteroaryl systems seemed a highly promising route to deliver the I-125 enriched **7** from the aryl bromide **5** (Supplementary Scheme 3; ref. 41). In our hands, this method for radiohalogenation was unsuccessful, presumably due to the structural sophistication

of **5** with several potential heteroatoms available for copper chelation. However, treatment of **5** with [¹²⁵I]NaI/chloramine T successfully delivered **7** with a radiochemical yield of 20% and a specific activity of 1.0 $\mu\text{Ci}/\mu\text{g}$ (¹²⁵I $T_{1/2}$ = ~60 d).

Concurrently, Raji cells (human B-cell lymphoma), which abundantly express $\alpha_4\beta_1$ integrin (16), were cultured, centrifuged, and injected into 11 female BALB/c nude mice. These xenograft tumors were allowed to grow to 50 to 200 mm. The I-125 analogue **7** was then injected into the tail vein, with animals sacrificed and organs and tumors removed, weighed, and counted after 24 and 48 hours. Although only one dose formulation was given and dose injections were performed at the same time in an identical manner for all mice, the blood clearance and biodistribution data allowed us to separate the mice into two groups: one with slow blood clearance and one with fast blood clearance (Supplementary Figs. S1 and S2). Three mice showed slow clearances (two mice at 24 h and one mouse at 48 h). These mice had approximately 15% still circulating in the blood thus providing high tumor uptakes of >6% ID/g. The liver, spleen, and marrow uptakes were <8% ID/g at 48 hours. However, five mice (three mice at 24 h and two mice at 48 h) showed that **7** was cleared rapidly from the blood and body. The major dose (25% ID/g) was mainly accumulated in the liver, spleen, and marrow, whereas the tumor uptake of these mice was very low (<1.5% ID/g).

Although these preliminary data have low statistical significance, we believe these results warrant further discussion and might be due to one or more factors. The radioiodo analogue **7**, having reduced *in vitro* affinity for $\alpha_4\beta_1$ integrin by nearly 10-fold compared with bromo analogue **5**, may have decreased *in vivo* affinity and selectivity. The iodobenzamidyl moiety of **7** might also be metabolically degraded, as seen with *p*-radioiodobenzamide derivatives (42, 43). Although we did not see *in vitro* peptide aggregation of **7**, it has been reported that the fast clearance patterns might be due to *in vivo* aggregation resulting in ineffective tumor targeting (44).

Radioiodination via electrophilic aromatic substitution

In addition to these mixed *in vivo* results (Supplementary Figs. S1 and S2), **7** was difficult to prepare in high radiochemical yield and crude purity. This provided the impetus for the synthesis of 3-radioiodotyrosine-derivative **8**, as tyrosine residues are rapidly radioiodinated with high regio- and chemoselectivity (21, 45). Moreover, previous optical conjugates **1**-Cy5.5 and **2**-Cy5.5 showed that the primary amide was successfully modified to a secondary amide without affecting activity, potency, or selectivity (3, 12, 14–16). With this in mind, Rink amide resin was first swollen in DMF for 3 hours, followed by Fmoc-deprotection and *N*-acylation with semi-orthogonally protected tyrosine to deliver the tyrosylated resin **16** (Supplementary Scheme 2). This resin was further elaborated into the bromobenzimidazole tetrapeptide **17** through analogous chemistry (Supplementary Scheme 2) and further elaborated elsewhere (15). This tyrosine derivative **17** was then rapidly radioiodinated using I-125-enriched sodium iodide with iodogen as an oxidant to afford the 3-radioiodo tyrosine derivative **8** in 90% radiochemical yield and with a specific activity of 2 $\mu\text{Ci}/\mu\text{g}$. Unfortunately, **8** performed poorly in *in vitro*

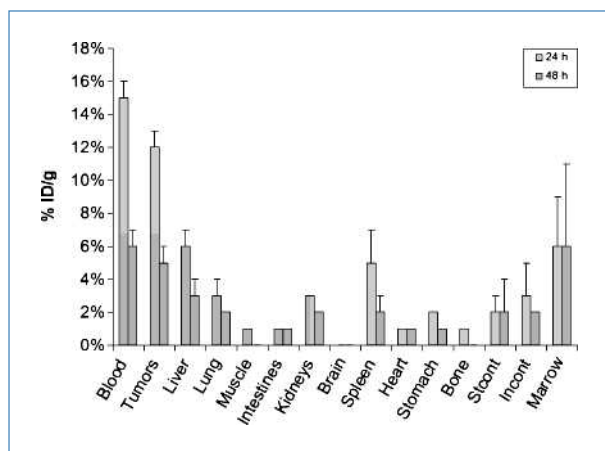


Figure 4. *Ex vivo* radio uptake data of **18** for various tumors and organs.

binding studies (<4%) and thus *in vivo* studies were not pursued. However, these *in vitro* results should not necessarily be viewed detrimentally; the *o*-hydroxyl group has been known to weaken the carbon-iodine bond and radioiodotyrosine derivatives have been known to undergo *in vivo* degradation due to their structural similarities to thyroid hormones (46).

Radioiodination via succinimidyl ester chemistry and biodistribution studies

Attention was then turned towards the synthesis of 4-radioiodobenzamidolysine-derivative **18**, as the bulkiness of the iodotyrosine may contribute to the poor *in vitro* binding. Rink amide resin was first swollen in DMF for 3 hours, followed by Fmoc-deprotection and *N*-acylation with Fmoc-Lys(Dde)-OH to deliver resin **19** (Fig. 3). Resin **19** was further elaborated into resin **20** through analogous chemistry (Supplementary Scheme 2) and described elsewhere (15). *N*-acylation of **20** with Fmoc-Lys(Alloc)-OH was followed by Fmoc-deprotection, and then coupling with bromobenzimidazole acid **5**. Alloc deprotection, followed by *N*-acylation with *trans*-3-(3-pyridyl)acrylic acid, Dde deprotection, and trifluoroacetic acid cleavage yielded **21**. The lysinated bromobenzimidazole **21** was radioiodinated by coupling the free amine of the lysine with the NHS-ester of I-125 enriched 4-iodobenzoic acid [prepared from *p*-aminobenzoic acid as outlined by Khalaj and colleagues (47)] to afford the 4-radioiodobenzamidolysine derivative **18** in 47% radiochemical yield and with a specific activity of 1.7 $\mu\text{Ci}/\mu\text{g}$.

To study the preliminary biodistribution of **18**, Raji cells (human B-cell lymphoma) expressing $\alpha_4\beta_1$ integrin were cultured, centrifuged, and injected into six nude mice. These xenograft tumors were grown to 50 to 200 mm. The I-125 analogue **18** was then injected into the tail vein, with half of the animals being sacrificed after 24 and 48 hours. As shown in Fig. 4, the organs and tumors were removed and counted with **18** having good tumor uptake ($12 \pm 1\%$ ID/g at 24 h and $4.5 \pm 1\%$ ID/g at 48 h) and minimal uptake in other organs. In particular, the low kidney uptake [tumor/kidney($t = 24$ h) $\sim 4:1$; tumor/kidney($t = 48$ h) $\sim 2.5:1$] was encouraging as this, in this initial assessment, has shown that radiolabeledazole analogue **18** might be a promising payload-ligand conjugate for targeting activated $\alpha_4\beta_1$ integrin-expressed tumors.

Conclusion

The results presented have shown the importance of advancing leads to target cancerous but not normal cells by exploiting the conformational differences of $\alpha_4\beta_1$ integrin. The

synthesis of azole heterocycles, which previously required harsh reaction conditions, long reaction times, and highly toxic reagents, can now be rapidly prepared through microwave-mediated synthesis using safer reagents with minimal purification. This report also provides an excellent example of how molecular models could be used as a guide to predict analogues that will have high affinity and to understand key weak force interactions. The potency of this unique class of compounds is likely attributed to a key aryl halide-hydrogen bond between the halobenzimidazole moiety and the primary amide side chain of Asn¹⁶¹ in the α_4 subunit. In preliminary studies, the condensed radioiodobenzimidazole analogue **18** has shown that a low tumor/kidney ratio may be achievable with a covalently attached radiolabeled modality, while minimizing the size and cost of the payload-ligand conjugate. These halobenzimidazoles are particularly attractive as this allows for the design of highly condensed ligand-payload conjugates for radiotherapeutic (I-131) and radiodiagnostic (F-18) agents for selectively detecting and treating T- and B-cell lymphomas that express $\alpha_4\beta_1$ integrin. Additionally, the bromo analogue **5** could provide valuable molecular insights into the binding site and integrin structure through photoaffinity cross-linking/mass spectroscopy (1:1 ⁷⁹Br:⁸¹Br) as well as cocrystallization X-ray studies (heavy atom effect).

Disclosure of Potential Conflicts of Interest

No potential conflicts of interest were disclosed.

Acknowledgments

Assistance with data compilation by Gary Mirick (U.C. Davis Cancer Center) is duly acknowledged.

Grant Support

National Cancer Institute (U19CA113298), National Science Foundation (CHE-0614756), National Institute for General Medical Sciences (ROI-GM076151), American Chemical Society's Division of Medicinal Chemistry Predoctoral Fellowship sponsored by Sanofi-Aventis (R.D. Carpenter), Howard Hughes Medical Institute Med into Grad Fellowship (R.D. Carpenter), U.C. Davis R.B. Miller Graduate Fellowship and Outstanding Dissertation Award (R.D. Carpenter), Alfred P. Sloan Minority Ph.D. Program (D.M. Solano), and U.C. Davis Alliance for Graduate Education and the Professoriate Advantage Program (D.M. Solano). NMR spectrometers were funded in part by the National Science Foundation (CHE-0443516 and CHE-9808183). A portion of this work was performed under the auspices of the U.S. Department of Energy by Lawrence Livermore National Laboratory under contract DE-AC52-07NA27344.

The costs of publication of this article were defrayed in part by the payment of page charges. This article must therefore be hereby marked *advertisement* in accordance with 18 U.S.C. Section 1734 solely to indicate this fact.

Received 10/08/2009; revised 03/27/2010; accepted 04/29/2010; published OnlineFirst 06/08/2010.

References

- Hait WN. Targeted cancer therapeutics. *Cancer Res* 2009;69:1263–7.
- Shimaoka M, Takagi J, Springer TA. Conformational regulation of integrin structure and function. *Annu Rev Biophys Biomol Struct* 2002;31:485–516.
- Peng L, Liu R, Marik J, Wang X, Takada Y, Lam KS. Combinatorial chemistry identifies high-affinity peptidomimetics against $\alpha_4\beta_1$ integrin for *in vivo* tumor imaging. *Nat Chem Biol* 2006;2:381–9.
- Martin KH, Slack JK, Boerner SA, Martin CC, Parsons T. Integrin connections map: to infinity and beyond. *Science* 2002;296:1652–3.
- Yusuf-Makagiansar H, Anderson ME, Yakovleva TV, Murray JS, Siahhan TJ. Inhibition of LFA-1/ICAM-1 and VLA-4/VCAM-1 as a

- therapeutic approach to inflammation and autoimmune diseases. *Med Res Rev* 2002;22:146–67.
6. Vincent AM, Cawley JC, Burtham J. Integrin function in chronic lymphocytic leukemia. *Blood* 1996;87:4780–8.
 7. Marco RA, Diaz-Montero CM, Wygant JN, Kleiner ES, McIntyre BW. α_4 integrin increases anoikis of human osteosarcoma cells. *J Cell Biochem* 2003;88:1038–47.
 8. Matsunaga T, Takemoto N, Sato T, et al. Interaction between leukemic-cell VLA-4 and stromal fibronectin is a decisive factor for minimal residual disease of acute myelogenous leukemia. *Nat Med* 2003;9:1158–65.
 9. Olson DL, Burkly LC, Leone DR, Dolinsky BM, Lobb RR. Anti- α_4 integrin monoclonal antibody inhibits multiple myeloma growth in a murine model. *Mol Cancer Ther* 2005;4:91–9.
 10. Garmy-Susini B, Jin H, Zhu Y, Hwang R, Varner J. Integrin $\alpha_4\beta_1$ -VCAM-1-mediated adhesion between endothelial and mural cells is required for blood vessel maturation. *J Clin Invest* 2005;115:1542–51.
 11. Jin H, Su J, Garmy-Susini B, Kleeman J, Varner J. Integrin $\alpha_4\beta_1$ promotes monocyte trafficking and angiogenesis in tumors. *Cancer Res* 2006;66:2146–52.
 12. Park SI, Manat R, Vikstrom B, et al. The use of one-bead one-compound combinatorial library method to identify peptide ligands for $\alpha_4\beta_1$ integrin receptor in non-Hodgkin's lymphoma. *Lett Pept Sci* 2002;8:171–8.
 13. Carpenter RD, Andrei M, Lau EY, et al. Highly potent, water soluble benzimidazole antagonist for activated $\alpha_4\beta_1$ integrin. *J Med Chem* 2007;50:5863–7.
 14. Peng L, Liu R, Andrei M, Xiao W, Lam KS. *In vivo* optical imaging of human lymphoma xenograft using a library-derived peptidomimetic against $\alpha_4\beta_1$ integrin. *Mol Cancer Ther* 2008;7:432–7.
 15. Carpenter RD, Andrei M, Lau EY, et al. Selectively targeting T- and B-cell lymphomas: a benzothiazole antagonist for $\alpha_4\beta_1$ integrin. *J Med Chem* 2009;52:14–9.
 16. DeNardo SJ, Liu R, Albrect H, et al. ^{111}In -LLP2A-DOTA polyethylene glycol-targeting $\alpha_4\beta_1$ integrin: comparative pharmacokinetics for imaging and therapy of lymphoid malignancies. *J Nucl Med* 2009;50:625–34.
 17. Aina OH, Liu R, Sutcliffe JL, Marik J, Pan C-X, Lam KS. From combinatorial chemistry to cancer-targeting peptides. *Mol Pharm* 2007;4:631–51.
 18. Perkins JJ, Zartman AE, Meissner RS. Synthesis of 2-(alkylamino) benzimidazoles. *Tetrahedron Lett* 1999;40:1103–6.
 19. Katritzky AR, Witek RM, Rodriguez-Garcia V, et al. Benzotriazole-assisted thioacylation. *J Org Chem* 2005;70:7866–81.
 20. de la Fuente MT, Casanova B, Garcia-Gila M, Silva A, Garcia-Pedro A. Fibronectin interaction with $\alpha_4\beta_1$ integrin prevents apoptosis in B-cell chronic lymphocytic leukemia: correlation with Bcl-2 and Bax. *Leukemia* 1999;13:266–74.
 21. Kersemans V, Cornelissen B, Kersemans K, et al. Comparative biodistribution study of the new tumor tracer [^{123}I]-2-iodo-L-phenylalanine with [^{123}I]-2-iodo-L-tyrosine. *Nucl Med Biol* 2006;33:111–7.
 22. Xiao T, Takagi J, Collier BS, Wang JH, Springer TA. Structural basis for allostery in integrins and binding of fibrinogen-mimetic therapeutics. *Nature* 2004;432:59.
 23. Margelevicius M, Venclovas C. PSI-BLAST-ISS: an intermediate sequence search tool for estimation of the position-specific alignment reliability. *BMC Bioinformatics* 2005;6:185.
 24. Altschul SF, Madden TL, Schaffer AA, et al. Gapped BLAST and PSI-BLAST: a new generation of protein database search programs. *Nucleic Acids Res* 1997;25:3389.
 25. Sali A, Blundell TL. Comparative protein modeling by satisfaction of spatial restraints. *J Mol Biol* 1993;234:779.
 26. Morris GM, Goodsell DS, Halliday RS, et al. Automated docking using a Lamarckian genetic algorithm and an empirical binding free energy function. *J Comput Chem* 1998;19:1639.
 27. Jackalian A, Jack DB, Bayly CI. Fast, efficient generation of high-quality atomic charges. AM1-BCC model: II. parameterization and validation. *J Comput Chem* 2002;23:1623.
 28. Weiner SJ, Kollman PA, Case DA, et al. A new force field for molecular simulation of nucleic acids and proteins. *J Am Chem Soc* 1984;106:765.
 29. Legge GB, Morris GM, Sanner MF, Takada Y, Olson AJ, Grynspan F. Model of the α L β 2 integrin I-domain/ICAM-1 DI interface suggest that subtle changes in loop orientation determine ligand specificity. *Proteins: Struct Funct Genet* 2002;48:151.
 30. Carpenter RD, DeBerdt PB, Lam KS, Kurth MJ. A carbodiimide-based library method. *J Comb Chem* 2006;8:907–14.
 31. Carpenter RD, Lam KS, Kurth MJ. Microwave-mediated heterocyclization to benzimidazo[2,1-b]quinazolin-12(5*H*)-ones. *J Org Chem* 2007;72:284–7.
 32. Carpenter RD, Fetting JC, Lam KS, Kurth MJ. Asymmetric catalysis: polystyrene-bound hydroxypropylthreonine in the enamine-mediated preparation of chromanones. *Angew Chem* 2008;120:6507–10; *Angew Chem Int Ed* 2008;47:6407–10.
 33. Biotage microwave conversion chart. Available from: <http://www.biotage.com/DynPage.aspx?id=21996>.
 34. Martin EJ, Critchlow RE. Beyond mere diversity: tailoring combinatorial libraries for drug discovery. *J Comb Chem* 1999;1:32–45.
 35. Lu Y, Yong W, Xu Z, et al. C-X...H contacts in biomolecular systems: how they contribute to protein-ligand binding affinity. *J Phys Chem B* 2009;113:12615–21.
 36. Auffinger P, Hays FA, Westhof E, Ho PS. Halogen bonds in biological molecules. *Proc Natl Acad Sci U S A* 2004;101:16789–94.
 37. Tawarada R, Seio K, Sekine M. Synthesis and properties of oligonucleotides with iodo-substituted aromatic aglycons: investigation of possible halogen bonding base pairs. *J Org Chem* 2008;73:383–90.
 38. Peet JH. How big is an atom? *Phys Educ* 1975:508–10.
 39. Kiyono Y, Kanegawa N, Kawashima H, Kitamura Y, Iida Y, Saji H. Evaluation of radioiodinated (*R*)-*N*-methyl-3-(2-iodophenoxy)-3-phenylpropanamine as a ligand for brain norepinephrine transporter imaging. *Nucl Med Biol* 2004;31:147–53.
 40. Araujo EB, Santos JS, Colturato MT, Muramoto E, Silva CPG. Optimization of a convenient route to produce *N*-succinimidyl 4-radiodobenzoate for radioiodination of proteins. *Appl Radiat Isot* 2003;58:667–73.
 41. Klapers A, Buchwald SL. Copper-catalyzed halogen exchange in aryl halides: an aromatic Finkelstein reaction. *J Am Chem Soc* 2002;124:14844–5.
 42. Garg PK, Slade SK, Harrison CL, Zalutsky MR. Labeling proteins using aryl iodide acylation agents: influence of *meta* vs *para* substitution on *in vivo* stability. *Nucl Med Biol* 1989;16:669–73.
 43. Wilbur DS, Hamlin DK, Chyan M-K, Kegley BB, Quinn J, Vessella RJ. Biotin reagents in antibody pretargeting. 6. Synthesis and *in vivo* evaluation of astatinated and radioiodinated aryl- and *nido*-carbonyl-biotin derivatives. *Bioconjug Chem* 2004;15:601–16.
 44. Yoshimoto M, Ogawa K, Washiyama K, et al. $\alpha_4\beta_3$ Integrin-targeting radionuclide therapy and imaging with monomeric RGD peptide. *Int J Cancer* 2008;123:709–15.
 45. Fernandes C, Oliveira C, Gano L, Bourkoulas A, Pirmettis I, Santos I. Radioiodination of new EGFR inhibitors as potential SPECT agents for molecular imaging of breast cancer. *Bioorg Med Chem* 2007;15:3974–80.
 46. Smallridge RC, Burman KD, Ward KE, et al. 3',5'-Diiodothyronine to 3'-monoiodothyronine conversion in the fed and fasted rat: Enzyme characteristics and evidence for two distinct 5'-deiodinases. *Endocrinology* 1981;108:2336–45.
 47. Khalaj A, Beiki D, Rafiee H, Najafi R. A new and simple synthesis of *N*-succinimidyl-4-[$^{127/125}\text{I}$]iodobenzoate involving a microwave-accelerated iodination step. *J Labelled Comp Radiopharm* 2001;44:235–40.

Cancer Research

The Journal of Cancer Research (1916–1930) | The American Journal of Cancer (1931–1940)

Halogenated Benzimidazole Carboxamides Target Integrin $\alpha_4\beta_1$ on T-Cell and B-Cell Lymphomas

Richard D. Carpenter, Arutselvan Natarajan, Edmond Y. Lau, et al.

Cancer Res 2010;70:5448-5456. Published OnlineFirst June 8, 2010.

Updated version Access the most recent version of this article at:
doi:[10.1158/0008-5472.CAN-09-3736](https://doi.org/10.1158/0008-5472.CAN-09-3736)

Supplementary Material Access the most recent supplemental material at:
<http://cancerres.aacrjournals.org/content/suppl/2010/06/07/0008-5472.CAN-09-3736.DC1.html>

Cited Articles This article cites by 45 articles, 9 of which you can access for free at:
<http://cancerres.aacrjournals.org/content/70/13/5448.full.html#ref-list-1>

E-mail alerts [Sign up to receive free email-alerts](#) related to this article or journal.

Reprints and Subscriptions To order reprints of this article or to subscribe to the journal, contact the AACR Publications Department at pubs@aacr.org.

Permissions To request permission to re-use all or part of this article, contact the AACR Publications Department at permissions@aacr.org.